Compensation On-line of Errors Caused by Rotor Centrifugal Deformation for a Magnetically Suspended Sensitive Gyroscope

Chao-Jun Xin*, Yuan-Wen Cai*, Yuan Ren[†] and Ya-Hong Fan**

Abstract – The aim of this paper is to design a centrifugal deformation error compensation method with guaranteed performance that allows angular velocity measurement of the magnetically suspended sensitive gyroscopes (MSSGs). The angular velocity measurement principle and the structure of the MSSG are described, and the analytical model of errors caused by MSSG rotor centrifugal deformation is established. Then, an on-line rotor centrifugal deformation error compensation method based on measurement of rotor spinning speed in real-time has been designed. The common issues caused by centrifugal deformation of spinning rotors can be effectively resolved by the proposed method. Comparative experimental results before and after compensation demonstrate the validity and superiority of the error compensation method.

Keywords: Magnetically suspended sensitive gyroscope (MSSG), Attitude angular measurement, Rotor centrifugal deformation, Error compensation, Analytical model

1. Introduction

In recent years, due to the advantages of zero friction, high-speed operation and low energy consumption, noncontact suspension technology is widely applied in space missions, such as highly accurate MSCMGs, flywheels, inertial guidance instruments, etc [1-5].

The suspension inertial systems, as electrostatic suspended gyroscopes and superconducting suspension gyroscopes, usually consist of a spinning hollow spherical rotor in a vacuum housing [6, 7] to insulate the disturbing torques. However, during the high speed rotation of the spherical rotor, there exist disturbing torques acting on the rotor, which is mainly the result of the centrifugal deformation of the rotor. And the centrifugal deformation is one of the main factors that produce the drift errors and decrease the accuracy of the measurement in dynamical situation for suspension inertial systems [8].

Aiming to compensation the errors caused by centrifugal deformation in suspension systems, many researchers have studied and analyzed the centrifugal deformation of rotors spinning at high speed. Due to lack of effective detecting means of rotor centrifugal deformation especially at high speed, researchers trend to study the elementary deformation laws and its effects with finite element method [8-10]. They have obtained perfect theoretical results about rotor centrifugal deformations, but they did not consider the compensation of measurement error produce by the rotor centrifugal deformation. Tang Jiqiang studies the stress and deformation of the superconducting suspension rotor subjected to centrifugal loads, and gains the theorical model of the centrifugal deformation for axisymmetric discal rotor [11]. Zhang Junan figures out that the rotor centrifugal deformation of electrostatic suspended gyroscope can produce a great impact on the measurement accuracy, and the disadvantages could be reduced by grinding the rotor on several atmospheres [12]. Liu Ruige [13] and Sun Xinmin [14] establishes the deformation formula produced by centrifugal load for the hollow spherical rotor in electrostatic suspended gyroscope individually. To eliminate the aspherical errors caused by centrifugal deformation qualitatively, they designs the hollow rotor to be a prolate sphere. In this way, the hollow rotor would transform to be an approximately ideal sphere under its specific spinning speed due to centrifugal deformation.

We can find that these existing studies can improve the measurement accuracy of suspension inertial systems to a certain extent. Because there is no credible theoretical model of disturbing torques generated from centrifugal deformation, their compensation method is only applicable to specific work conditions, but not to universal conditions at different rotor spinning speed.

In this paper, a magnetically suspended sensitive gyroscope is developed for angular velocity measurement. The complicated structure rotor with spherical envelope surfaces is levitated by four electromagnetic bearings in the center of the housing, and spinning at high spinning speed [15, 16]. In order to compensate the measurement error induced by rotor centrifugal deformation, thus improve the attitude measurement accuracy of a MSSG, the analytical expression of the disturbing torques caused by deformation has been deduced. And a universal method to compensate the centrifugal deformation on line for devices with

† Corresponding Author: Dept. of Space Science and Technology, Space Engineering University, China.(jingninan@126.com)
* Dept. of Space Science and Technology, Space Engineering University, China.
** Institute of Control Engineering, Beijing, China.

spinning rotors has been proposed.

The remainder of this paper is organized as follows. In Section 2, the structure of the MSSG and the measurement principle are introduced. Next, the rotor centrifugal deformation is modeled and analyzed, and the model of the measurement error caused by rotor centrifugal deformation has been established in Section 3. In section 4, the compensation method for deformation error has been brought forward, and section 5 conducts the comparative simulations to testify the measurement performance with the proposed compensation method. Follow on, Section 6 concludes this paper.

2. Angular Velocity Measurement Principle of a MSSG

2.1 Composition of a MSSG

The MSSG studied in this paper consists of rotor, stator, high speed motor, torquer, a gyro house and displacement sensors et al. Fig. 1(a) shows the main configuration of the MSSG.

The rotor of the MSSG is a type of spherical in structure, which is made of magnetic material in whole. Radiuses of rotor in axial and radial are different, while the radius is r_1 in radial and r_2 in axial. Both the magnetic pole envelope surfaces (MPES) of stator and rotor in axial and radial are spherical surfaces.

The rotor is levitating in the center of the stator cavity by magnetic pull produced from the interaction of the electromagnetic stator and the rotor. The torquer is a Lorentz Force Magnetic Bearing (LFMB), which is used to control the tilting of the rotor. Permanent magnets of LFMB are installed in the outer rim of the gyro rotor, and its windings are stickled on the torquer framework symmetrically. The tilting angles of rotor are measured by the axial and radial displacement sensors. And the rotation of the rotor is driven by a hollow cup permanent magnet brushless DC motor, whose windings are cured on the frame of the cup-chapped motor stator. The motor magnets are installed in the inner rim of the gyro rotor with six poles structure.

Due to the rims in the MSSG rotor and the its different radiuses in axial and radial, it was machined to be an complicated configuration, as is shown in Fig. 1(b). When the MPESs of the rotor are ideal spherical surfaces, the magnetic forces over the entire surface of the rotor magnetic poles will pass through its geometric center and no torques acting on the rotor. However, when the MPESs deflected from the ideal spherical surfaces, the disturbing torques would appear and act on the rotor, then the drift angular velocity comes up.

### 2.2 Principle of attitude angular measurement

In the rotor coordinate system (x, y, z), O is defined as the geometric center of rotor, and also the origin of the rotor coordinate system. The axes are defined to be aligned with the principal axes of inertia of rotor. And Ω is the spinning speed of the rotor around the major axis of inertia, z-axis. Origin of the stator coordinate system (X, Y, Z) is the center of the stator cavity.

When the gyro-carrier is static and the MPESs are ideal spherical, the rotor is levitating in the center of the gyro house, spinning about z-axis at angular rate Ω. However, when the gyro-carrier fixed with the gyro house comes into an off-axis attitude angular rate ω_{ib} related to the inertial space, the attitude of levitating rotor would remain the same dues to the gyroscopic inertia of the rotor. The displacement sensors would pick up the position changes of the rotor related to gyro house, and transmit the signals to control system. Control current will be applied to the windings of the torquer by the control system according to the signals, compelling the rotor promptly rotate back to its equilibrium position in gyro house at angular rate ω_{ir} related to the inertial space.

The control bandwidth of the torquer and the measurement bandwidth of the displacement sensors are much higher than the attitude change frequency of the gyro-carrier, so within the control bandwidth, the rotor would always track the angular velocity of the gyro-carrier in x- and y-axes, stabilizing the rotor at the predesigned
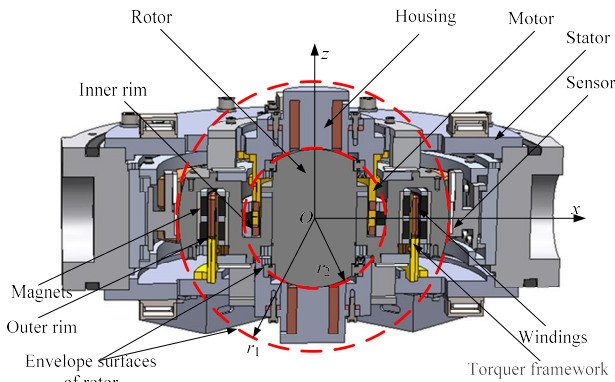
(a) Configuration of the MSSG
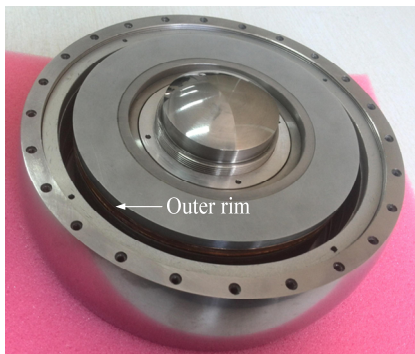
(b) Rotor of the MSSG

Fig. 1. Configuration of the MSSG and its rotor

equilibrium position.

Angular velocity of the gyro-carrier can be described as

$$\boldsymbol{\omega}_{ib} = \boldsymbol{\omega}_{ir} - \boldsymbol{\omega}_{rb} \tag{1}$$

where $\boldsymbol{\omega}_{rb}$ is the deflection angular velocity of rotor related to the gyro house. By using Euler dynamic equations, the equivalent moment acting on the rotor in x- and y-directions as the gyro-carrier rotating can be obtained as

$$\begin{cases} M_x = J_z \Omega \omega_{iby} + J_r \dot{\omega}_{ibx} \\ M_y = -J_z \Omega \omega_{ibx} + J_r \dot{\omega}_{iby} \end{cases} \tag{2}$$

where J_z is the polar moment of inertia of the rotor, and J_r is the equator moment of inertia of the rotor, ω_{ibx} and ω_{iby} is the angular velocity of gyro-carrier around x- and y-axes, respectively. M_x and M_y are torques acting on the rotor around x- and y-axes.

When the angular acceleration of the gyro-carrier is small, the above formula can be turned into gyroscopic effect precession equation since $J_z \Omega \gg J_r$, and the angular velocity of the gyro-carrier can be formulated as

$$\begin{cases} \omega_{iby} = \dfrac{M_x}{J_z \Omega} \\ \omega_{ibx} = -\dfrac{M_y}{J_z \Omega} \end{cases} \tag{3}$$

Ideally, the structure of the MSSG has determined that the moments acting on the levitating rotor are generated only from the torquer.

3. Modeling and Analysis for Rotor Centrifugal Deformation

3.1 Errors from rotor asphericity

When the rotor MPESs in radial and axial are ideal spheres, the magnetic forces pass through the geometric center of the rotor, and there is no disturbing torque about the geometric center. And the rotor can suspend and spin steadily at the center of the stator. However, if the MPESs deviate from the ideal spheres and become torispherical

close surfaces due to the centrifugal force, the magnetic forces would not pass through the geometric center of the rotor any longer, and disturbing torque will generated by the magnetic force about the geometric center of the rotor.

Assumed the rotor MPES to be torispherical surface of revolution with radius r_1, and its radius vector in meridian plane can be described by Legendre polynomial series as

$$r_1(\theta_1) = r_{10} + \sum_{n=1}^{\infty} a_n P_n(\cos\theta_1) \tag{4}$$

where, r_{10} is the nominal radius of the ideal envelope surface, a_n is the aspheric coefficient of each harmonic in describing the envelope surface, θ_1 is the angle between r_1 and the spin axis of rotor. $P_n(\cos\theta_1)$ is the Legendre polynomial series which is written as

$$\begin{aligned} P_1(\cos\theta_1) &= \cos\theta_1 \\ P_2(\cos\theta_1) &= \frac{1}{2}(3\cos^2\theta_1 - 1) \\ P_{n+1}(\cos\theta_1) &= \frac{\begin{bmatrix} (2n+1)\cos\theta_1 P_n(\cos\theta_1) \\ -n P_{n-1}(\cos\theta_1) \end{bmatrix}}{n+1} \quad (n \geq 2) \end{aligned} \tag{5}$$

Hence the gap size between stator magnetic pole surface and the rotor can be written as Eq. (6). In Eq. (6), δ_0 is the nominal gap size, $\Delta\delta$ is the variation of δ_0, $\boldsymbol{e} = e_X \boldsymbol{X}_0 + e_Y \boldsymbol{Y}_0 + e_Z \boldsymbol{Z}_0$ is the linear displacement vector from O to the geometric center of rotor, named eccentricity, θ is the elevation while φ is the azimuth of a arbitrary point on the MPESs. And $\cos\theta_1$ can be written as Eq. (7), in which α, β, γ are the direction cosines of spinning axis of rotor in the stator coordinate system. And the final equation of the disturbing torques generated from six stator magnetic poles can be written as Eq. (8) [15], in which μ_0 is the magnetic permeability of vacuum, N is the turns of coil on the stator magnetic poles, I is the current in the coils, R_i is the nominal radius of the ith stator magnetic pole. S_i is the area of the ith stator magnetic pole which applied magnetic force on the rotor.

Under the action of the disturbing torque, the spinning axis of rotor will gradually deviated from its original position, resulting drift angular velocity. According to angular momentum law, the drift angular velocity can be expressed as Eq. (9).

$$\delta = \delta_0 + \Delta\delta = \delta_0 - \sum_{n=1}^{\infty} a_n P_n(\cos\theta_1) - e_X \sin\theta\cos\varphi - e_Y \sin\theta\sin\varphi - e_Z \cos\theta \tag{6}$$

$$\cos\theta_1 = \alpha \sin\theta\cos\varphi + \beta \sin\theta\sin\varphi + \gamma \cos\theta \tag{7}$$

$$\boldsymbol{T} = \sum_{i=1}^{6} \iint_{S_i} \frac{\mu_0 N^2 I^2 R_i^2}{8\delta_0^2} \cdot \left(1 - \frac{2\Delta\delta_i}{\delta_0}\right) \cdot \sum_{n=1}^{\infty} a_n P_n'(\cos\theta_1) \cdot \begin{bmatrix} \beta\cos\theta - \gamma\sin\theta\sin\varphi \\ \gamma\sin\theta\cos\varphi - \alpha\cos\theta \\ \alpha\sin\theta\sin\varphi - \beta\sin\theta\cos\varphi \end{bmatrix} d\theta d\varphi \tag{8}$$

$$\begin{bmatrix} \omega_x \\ \omega_y \\ \omega_z \end{bmatrix} = \frac{1}{H}\begin{bmatrix} 0 & \gamma & -\beta \\ -\gamma & 0 & \alpha \\ \beta & -\alpha & 0 \end{bmatrix}^{-1}\begin{bmatrix} T_x \\ T_y \\ T_z \end{bmatrix} \qquad (9)$$

where the angular momentum can be described with the polar moment of inertia of the rotor J as

$$H = J_z \cdot \Omega \qquad (10)$$

3.2 Description of rotor centrifugal deformation

In order to simplify the analysis of errors produced by centrifugal deformation of rotor, the following assumptions are made:

(1) The MPESs of stator and the rotor are ideal spherical surfaces under static condition, therefore there is no aspheric error.

(2) The rotor is a homogeneous and isotropic elastic structure, hence there is no static and dynamic mass unbalance.

(3) All the planes paralleled to equatorial plane in the rotor remain planar after centrifugal deformation.

Set a spherical coordinate frame(θ, ϕ, r), whose origin is the geometric center of the rotor after centrifugal deformation, as is shown in Fig. 2. Assuming that point P is on the MPES of the rotor, θ and r are the coordinate value of P in θ- and r-direction, respectively. ε_θ, ε_ϕ, ε_r and σ_θ, σ_ϕ, σ_r are the linear strain and normal stress in the three axes. E, ν are the Young modulus and Poisson's ratio of the rotor material. u, t, w are the projection of the displacement vector of point P in θ-, ϕ- and r-direction, respectively.

A volume element from the equatorial plane, decided by dr and dϕ is taken as research object, the equation of forces in radial can be written as Eq. (11). In which ρ is the density of the rotor material, b is the thickness of the volume element.

$$\sigma_r r b d\phi - (\sigma_r + d\sigma_r)(r+dr)bd\phi + \sigma_\phi b dr d\phi = \rho\Omega^2 r^2 b dr d\phi \qquad (11)$$
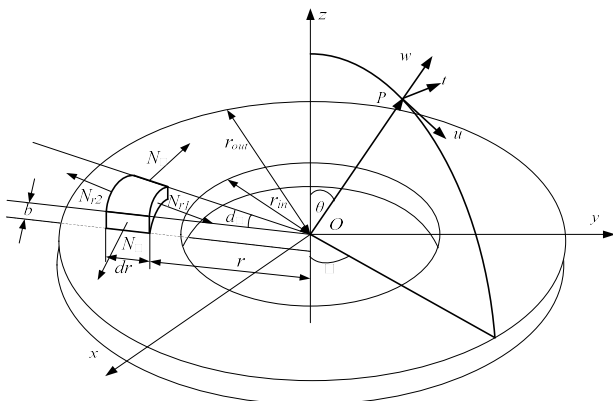

Fig. 2. Stress analysis of the volume element

According to assumption (3), by slicing the rotor with equal latitude planes we can acquire infinite thin discs paralleled to equatorial plane, whose top and bottom surfaces remain planar after centrifugal deformation. Therefore there is no angular strain among each discs. At the same time, there is no shear stress but normal stresses on the top and bottom surfaces of the discs. And the direction of the normal stresses σ_z on the top and bottom surfaces of the discs are perpendicular to their surfaces, thus the normal stresses have no influence on the equation of forces of the volume element in radial.

Based on the axial symmetry of the rotor configuration and its load, both the displacements u and t are zero. Considering the relationship between stress and displacement, Eq. (11) can be expressed as a differential equation about w,

$$r^2\frac{d^2w}{dr^2} + r\frac{dw}{dr} - w = -\frac{1-\nu^2}{E}\rho\Omega^2 r^3 \qquad (12)$$

The solution of the above equation is the radial deformation formula of the volume element disc at equatorial plane

$$w = \frac{\rho\Omega^2}{8E}\left[\begin{array}{l}(1-\nu)(3+\nu)\left(r_{out}^2+r_{in}^2\right)r + \dfrac{4\nu^2\left(r_{out}^2+r_{in}^2\right)r}{(2\nu+1)} \\ + \left(\dfrac{(3+\nu)(1+\nu)}{r}\right)r_{out}^2 r_{in}^2 - \left(1-\nu^2\right)r^3\end{array}\right] \qquad (13)$$

where r_{in} and r_{out} are the inner and outer radius, respectively.

Regarding the rotor as the superposition of the infinite volume element discs, and assuming there are no shear stresses but normal stresses among each discs, the above result could spread to the discs at any equal latitude planes, which can be written as

$$u_\rho = \frac{\rho\Omega^2(\nu+1)}{4E(2\nu+1)}\left[\left(r_{out}\sin\theta\right)^3 + (4\nu+3)r_{in}^2 r_{out}\sin\theta\right] \qquad (14)$$

where u_ρ is the radial deformation of the disc at $\left|\dfrac{\pi}{2}-\theta\right|$ equal latitude plane.

The same procedure may be easily adapted to obtain the axial deformation formula of the discs at any equal latitude planes, it is

$$u_z = \frac{(1+\nu)\rho\nu\Omega^2}{2E(2\nu+1)}\left(-r_{out}^3\cos\theta + \frac{1}{3}r_{out}^3\cos^3\theta - r_{in}^2 r_{out}\cos\theta\right) \qquad (15)$$

Therefore, the deformation of point P on the spherical rotor surface along its radius vector can be expressed as

Eq. (16). According the analysis in subsection 3.2, the MPES of a spherical rotor is a torispherical surface of revolution after centrifugal deformation, and its radius vector in meridian plane can be described by Legendre polynomial series. Transform Eq. (16) into the expression of Legendre polynomial series, we can get Eq. (17)

$$
w_a = \left[\frac{8-8\nu}{15} \right] k_r r_2^3 - \frac{(16+20\nu)}{21} k_r r_2^3 \left[\frac{3}{2}\cos^2\theta - \frac{1}{2} \right] + \frac{24+16\nu}{105} k_r r_2^3 \left[\frac{35}{8}\cos^4\theta - \frac{30}{8}\cos^2\theta + \frac{3}{8} \right]
\tag{20}
$$

$$
w = u_\rho\sin\theta + u_z\cos\theta = \rho\Omega^2 \frac{(\nu+1)}{4E(2\nu+1)} \left[\begin{array}{l} r_{out}^3 + (4\nu+3)r_{in}^2 r_{out} + \frac{3+2\nu}{3}r_{out}^3\cos^4\theta \\ -\left(2(1+\nu)r_{out}^2 + 3(2\nu+1)r_{in}^2\right)r_{out}\cos^2\theta \end{array} \right]
\tag{16}
$$

$$
w = \left[\frac{8-8\nu}{15} \right] k_r r_{out}^3 + (2\nu+2)k_r r_{out} r_{in}^2 - k_r \left[\frac{(16+20\nu)}{21}r_{out}^3 + (4\nu+2)r_{out}r_{in}^2 \right] \left[\frac{3}{2}\cos^2\theta - \frac{1}{2} \right] + \frac{24+16\nu}{105}k_r r_{out}^3 \left[\frac{35}{8}\cos^4\theta - \frac{30}{8}\cos^2\theta + \frac{3}{8} \right]
\tag{17}
$$

where

$$
k_r = \rho\Omega^2 \frac{(\nu+1)}{4E(2\nu+1)}
\tag{18}
$$

Obviously, the centrifugal deformation of a spherical rotor can be described in 4th harmonic, and the harmonic coefficients are

$$
\begin{aligned}
a_0 &= \left[\frac{8-8\nu}{15} \right] k_r r_{out}^3 + (2\nu+2)k_r r_{out} r_{in}^2 \\
a_1 &= 0 \\
a_2 &= -\left[\frac{(16+20\nu)}{21}k_r r_{out}^3 + (4\nu+2)k_r r_{out} r_{in}^2 \right] \\
a_3 &= 0 \\
a_4 &= \frac{24+16\nu}{105}k_r r_{out}^3
\end{aligned}
\tag{19}
$$

Modifying r_{in} into 0 in above equations, we can get the deformation of a solid spherical rotor along its radius vector.

3.3 Modeling of centrifugal deformation error for A MSSG

The structure of the MSSG rotor is a complicated, approximately spherical segment with multiple hollow grooves, and the radius of rotor envelope surfaces in axial and radial are different, as is shown in Fig. 3. Calculation of MSSG rotor centrifugal deformations can be fallen into two parts.

Firstly, calculate the rotor centrifugal deformation at axial magnetic pole. From Fig. 3, we can discover that axial magnetic pole of the rotor can be seen as two upper and bottom spherical crowns, and their centrifugal deformation can be easily figured up using Eq. (17) as

The centrifugal deformations of the top and bottom spherical crowns at the spinning speed of 10000rpm result from Eq. (20) are showing in Fig. 4. From Fig. 4 we can see that both the upper and bottom spherical crowns suffered a inward contraction, and the at the pole locations, w_a reaches its negative peak of -6.17×10^{-6}m.
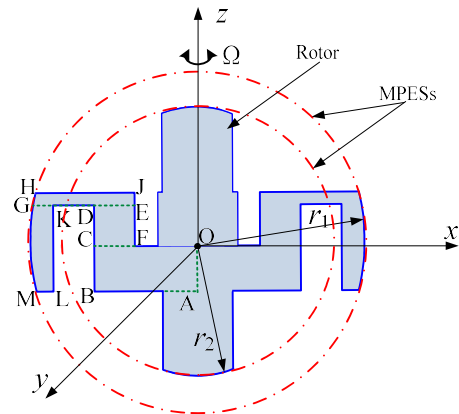

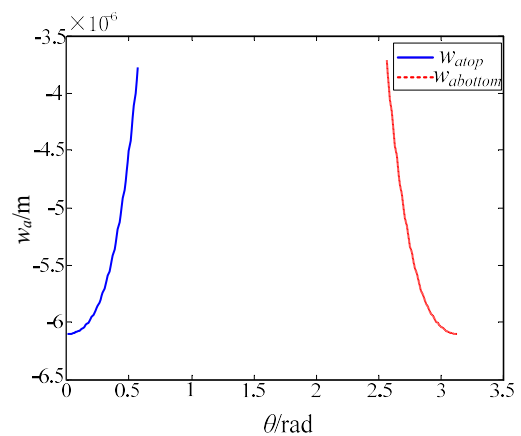**Fig. 3.** Computing method of rotor centrifugal deformation radially

Fig. 4. Centrifugal deformations of the MSSG rotor axially

Secondly, calculate the rotor centrifugal deformation at radial magnetic pole. Due to the complicated structure of the radial magnetic pole of the rotor, we neither calculate its centrifugal deformation as a solid spherical segment, nor as a hollow spherical segment. Having considered the above fact, an approximation method is designed as follow.

(1) Taking the rectangle ABCO as a cross-section, as is shown in Fig. 3, and rotating it about *z*-axis to generate a cylinder. Calculate the centrifugal deformation of the cylinder according Eq. (13).

(2) Taking the rectangle CDEF as a cross-section in Fig. 3, and rotating it about *z*-axis to generate a cylindrical ring. Calculate the centrifugal deformation of the cylindrical ring according Eq. (13), and taking the abscissa value of point F as the inner radius and the abscissa value of point B calculated in step (1) as the outer radius.

(3) Taking the rectangle GHJE as a cross-section in Fig. 3, and rotating it about *z*-axis to generate a cylindrical ring with spherical external surface. Calculate the centrifugal deformation of the cylindrical ring according Eq. (16), taking the abscissa value of point E calculated in step (2) as the inner radius, and taking the length of OG after centrifugal deformation of point E as the outer radius. The length of OG can be obtained as

$$\overline{OG} = \sqrt{\left(\sqrt{r_1^2 - z_G^2} + |\Delta x_E|\right)^2 + z_G^2} \tag{21}$$

where z_G is the coordinate value of point G in *z*-axis, Δx_E is the abscissa increment of point E after centrifugal deformation.

(4) Taking the rectangle MLKG as a cross-section in Fig. 3, and rotating it about *z*-axis to generate a cylindrical ring with spherical external surface. Calculate the centrifugal deformation of the cylindrical ring according Eq. (16), taking the abscissa value of point K calculated in step (3) as the inner radius, and the length of OG after centrifugal deformation of point G as the outer radius.

(5) In the end, centrifugal deformation of the radial magnetic pole of the rotor is composed of centrifugal deformations of the two cylindrical rings calculated in step (3) and (4). The deformation curves are revealed in Fig. 5. Due to the different thickness of the two

cylindrical rings, centrifugal deformations of the two parts are discontinuous. However, under the effect of bending moment, the centrifugal deformation is obliged to be continuous. Therefore, the upper ring with larger thickness reduces the centrifugal deformation of junction between the two rings. And with the increase of the distance to the upper ring, the effect of bending moment to lower one fades away. Connecting the two deformation curves and smoothed it, the rotor centrifugal deformation curve of the radial magnetic pole can be acquired, as is shown in Fig. 5. And by fitting the deformation curve, we can get the radial centrifugal deformation formula as Eq. (22).

$$w_r = \frac{(\nu+1)\rho\Omega^2}{4E(2\nu+1)}\left[a_0 + a_1\cos\theta + a_2\left[\frac{3}{2}\cos^2\theta - \frac{1}{2}\right]\right.$$
$$\left. + a_3\left[\frac{5}{2}\cos^3\theta - \frac{3}{2}\cos\theta\right] + a_4\left[\frac{35}{8}\cos^4\theta - \frac{30}{8}\cos^2\theta + \frac{3}{8}\right]\right] \tag{22}$$

$$\begin{aligned} a_0 &= 8.9516\times10^{-4} \\ a_1 &= -1.4839\times10^{-4} \\ a_2 &= -1.2\times10^{-3} \\ a_3 &= 9.6935\times10^{-4} \\ a_4 &= 5.1613\times10^{-5} \end{aligned} \tag{23}$$

$$\mathbf{T}_{deform} = \mathbf{T}_{deform\_a} + \mathbf{T}_{deform\_r} = \sum_{i=1}^{2}\iint_{S_i}\frac{\mu_0 N^2 I^2 R_2^2}{8\delta_0^2}\left(1 - \frac{2w_a}{\delta_0}\right)\cdot\sum_{n=1}^{\infty}a_n P_n'(\cos\theta_1)\times\begin{bmatrix}\beta_z\cos\theta - \gamma_z\sin\theta\sin\varphi \\ \gamma_z\sin\theta\cos\varphi - \alpha_z\cos\theta \\ \alpha_z\sin\theta\sin\varphi - \beta_z\sin\theta\cos\varphi\end{bmatrix}d\theta_1 d\varphi$$
$$+ \sum_{i=1}^{4}\iint_{S_i}\frac{\mu_0 N^2 I^2 R_1^2}{8\delta_0^2}\left(1 - \frac{2w_r}{\delta_0}\right)\cdot\sum_{n=1}^{\infty}a_n P_n'(\cos\theta_1)\times\begin{bmatrix}\beta_z\cos\theta - \gamma_z\sin\theta\sin\varphi \\ \gamma_z\sin\theta\cos\varphi - \alpha_z\cos\theta \\ \alpha_z\cos\theta\sin\varphi - \beta_z\sin\theta\cos\varphi\end{bmatrix}d\theta_1 d\varphi \tag{24}$$

From Eq. (8), we can conclude that the disturbing torque produce by the aspherical error is closely related to the variation of air gap, $\Delta\delta$. And according to the analysis in this subsection, we can see that the centrifugal deformations of MSSG rotor in radius vector direction
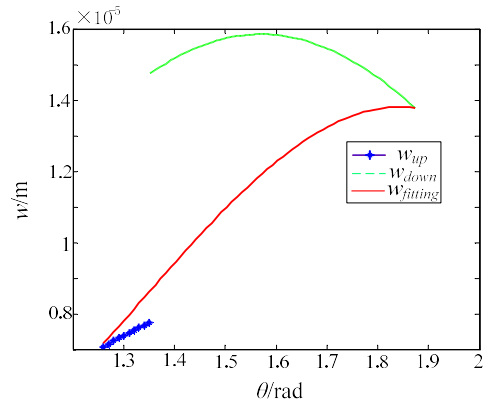

Fig. 5. Centrifugal deformations of the MSSG rotor radially

axially and radially, w_a and w_r, are just the value of air gap. The disturbing torque produce by centrifugal deformations of MSSG rotor $\mathbf{T}_{deform}$ can be written as Eq. (24), in which $\mathbf{T}_{deform\_a}$, $\mathbf{T}_{deform\_r}$ are the disturbing torques produced by centrifugal deformations of axial and radial part of MSSG rotor calculated according Eq. (22), respectively. Substituting Eq. (24) into (9), we can get the angular velocity error generated from centrifugal deformations of MSSG rotor as Eq. (25).

$$\begin{bmatrix} \omega_{dx} \\ \omega_{dy} \\ \omega_{dz} \end{bmatrix} = \frac{1}{H} \begin{bmatrix} 0 & \gamma & -\beta \\ -\gamma & 0 & \alpha \\ \beta & -\alpha & 0 \end{bmatrix}^{-1} \mathbf{T}_{deform} \qquad (25)$$

4. Design of Error Compensation

To effectively improve the measurement accuracy of the MSSG, the angular velocity error caused by centrifugal deformations of MSSG rotor has to be reduced. The method to compensate the centrifugal deformation error for the MSSG can be obtained on the basis of the above analysis. According to Eq. (22) and (24), it can be perceived that the disturbing torques can be acquired in real time by measuring the spinning speed of MSSG rotor on-line. The spinning speed of MSSG rotor can be measured by Hall switch sensors installed in the driven motor. Substituting the spinning speed of rotor into Eq. (22), the rotor centrifugal deformation radius vector direction can be obtained in real-time. Substituting the centrifugal deformation into Eq. (24), the disturbing torque caused by rotor centrifugal deformation may be received in real-time.

It is clear that, as a result of the centrifugal deformation of MSSG rotor, the control moment applied to rotor has contained the disturbing torque caused by rotor centrifugal deformation. In order to get the accurate angular velocity measured by the MSSG, we have to compensate the disturbing torque from the original control moment. The angular velocity after compensation can be expressed as

$$\begin{cases} \omega_{iby} = \dfrac{M_x - T_{deform\_x}}{J_z \Omega} \\ \omega_{ibx} = -\dfrac{M_y - T_{deform\_y}}{J_z \Omega} \end{cases} \qquad (26)$$

where, T_{deform_x}, T_{deform_y} are the projection of the disturbing torque caused by centrifugal deformation in x- and y-direction, respectively.

Fig. 6 reveals the schematic diagram of the error compensation method based on the above idea. The part drawing in real lines is the original angular velocity measuring method. T_m is the transfer function of torque converter, which transform the angular motion $\boldsymbol{\omega}_{ib}$ of the gyro-carrier into precession torque M_g. M_C is the control torque produced by the torquer according to the controller signals, whose transfer function is G_p. G_g is the transfer function of the rotor, and K_s is the model of displacement sensors. G_cG_w is the transfer function of gyro controller and amplifier, whose output could be picked by the current sensors modeled as K_I. The dashed box in Fig. 6 indicates the error compensation method to reduce the rotor centrifugal deformation error. By applying the real-time measured value of rotor spinning speed as the key resolving parameter, and transmitting it to model of rotor centrifugal deformation and model of disturbing torque, the high accuracy measured value of angular velocity can be acquired base on the improved measurement Eq. (26).

5. Numerical Simulation

In this section, the theoretical model accuracy of the MSSG rotor centrifugal deformation is validated based on finite element analysis method, and simulations of the proposed error compensation method is conducted to verify the satisfactory correction effect. All the simulations are put up on the assumption that there are no other disturbing torques come into being. The system parameters of the MSSG are shown in Table 1.
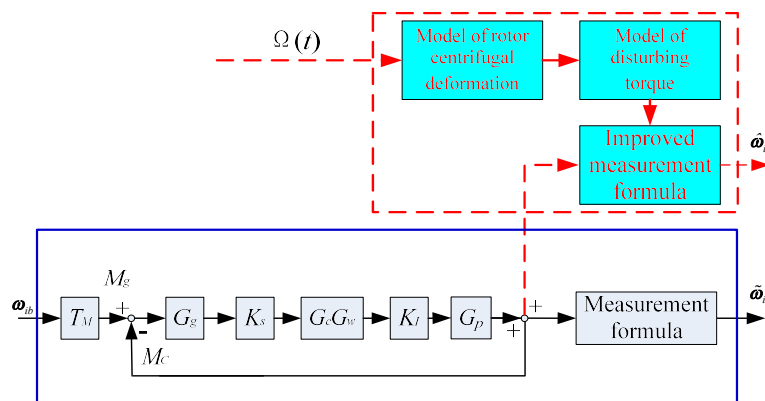

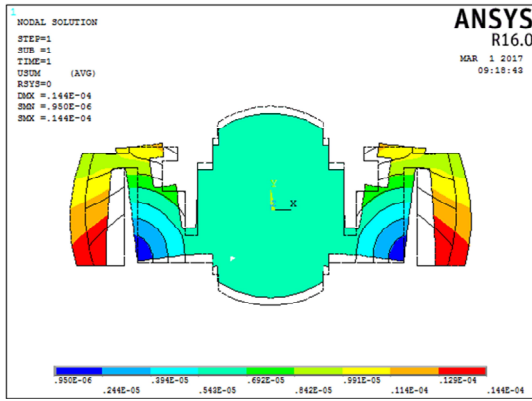**Fig. 6.** Schematic diagram of the error compensation method
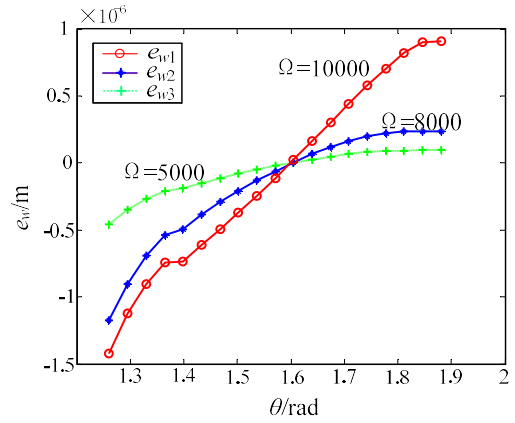
Fig. 7. FEM centrifugal deformation of MSSG rotor

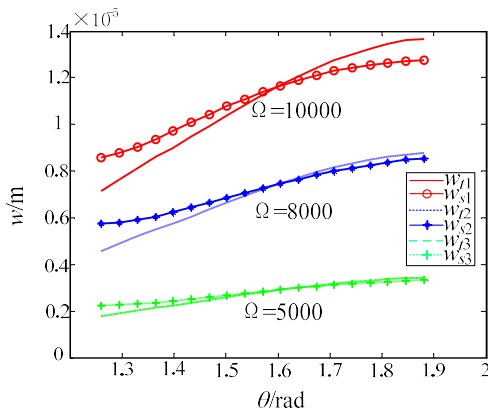**Fig. 8.** Comparison of theoretical results and FEM results

Table 1. System parameters of the MSSG

parameter (unit)	numerical value	parameter (unit)	numerical value
m (kg)	4.7	J_r ($kg \cdot m^2$)	0.0034
n_a	100	J_z ($kg \cdot m^2$)	0.0052
n_r	200	r_1 (m)	0.07865
δ_0 (m)	0.00035	r_2 (m)	0.041

Under the MSSG rotor angular velocity of 10000rpm, the MSSG rotor centrifugal deformation base on finite element analysis is shown in Fig. 7, the dotted lines delegate the outlines of the rotor before centrifugal deformation. As is shown in Fig. 7, owing to the high-speed revolution of the rotor, centrifugal deformation comes into being both in axial and radial of the rotor, and the maximum of the deformation appears at the lower edges, that is point B in Fig. 3, which is agree with the above theoretical analysis.

In order to confirm the validity of the centrifugal deformation computed from the theoretical model established in this paper, the comparative analysis between centrifugal deformations computed from theoretical model and simulation is carried out. The comparative results under different rotor spinning speed are shown in Fig. 8.

Fig. 9. Errors of theoretical results relative to FEM results

Fig. 10. Input angular velocities in x- and y-direction

According to Fig. 8, we can know that the rotor centrifugal deformations from theoretical model and simulation are same in trend under different rotor spinning speed, however the changes rate of theoretical calculation results are larger. At the location of small elevation, the theoretical results are less than the simulation results, but at the location of large elevation, the theoretical results are greater than the simulation results. At 10000rpm, the maximum of rotor centrifugal deformation are 1.35×10^{-5}m in theoretical and 1.30×10^{-5}m in simulation at the elevation of 1.88rad, and the minimum are 0.70×10^{-5}m in theoretical and 0.85×10^{-5}m in simulation at the elevation of 1.26rad. The relations between theoretical model and FEM simulation for axial MPEPs are approximately the same as the radial one, which are not dwelled on in this paper.

Fig. 9 shows the errors of theoretical results relative to simulation results. As it can be seen from Fig. 9, with the increase of the rotor spinning speed the relative errors become more and more obvious. And the maximums appear at the top edges of the radial magnetic pole of rotor, that is point H in Fig. 3. At 10000rpm, the maximal relative error is about 16%. The errors between theoretical and simulation results are mainly from: (1) the assumptions in rotor centrifugal deformation analysis; (2) the simplification of rotor structure in theoretical modeling;
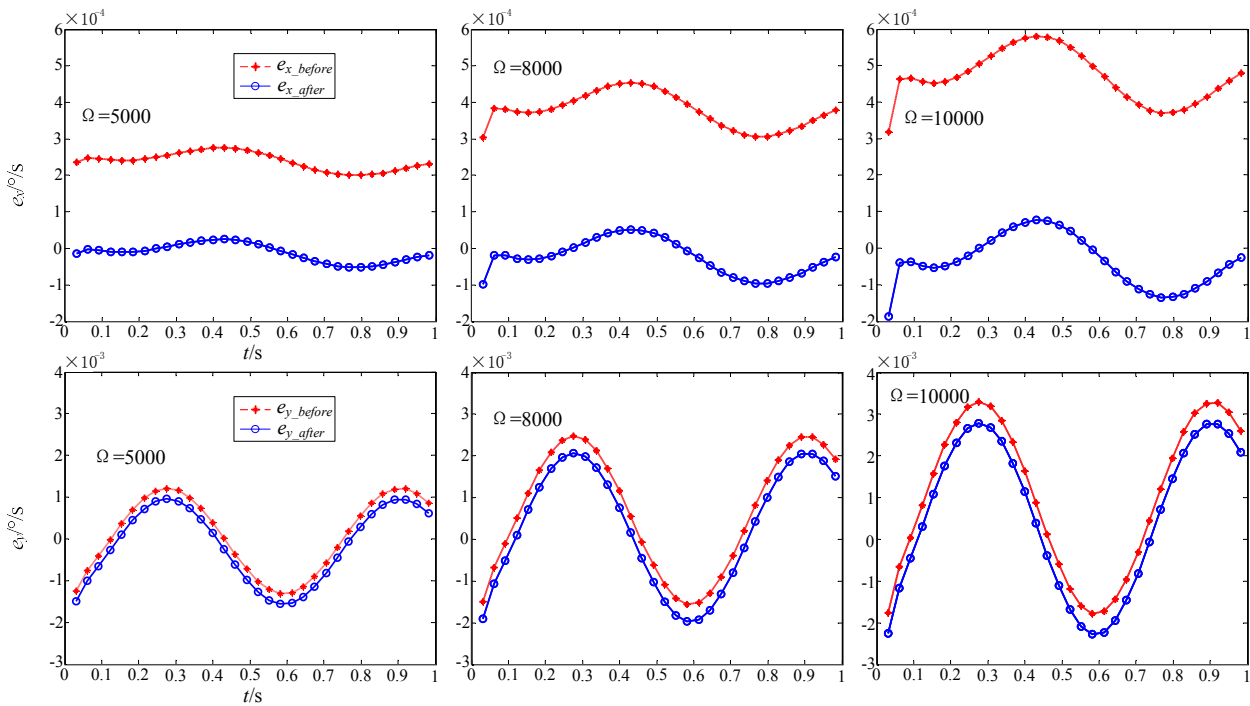
Fig. 11. Errors comparison before and after compensation

(3) the simplification in derivation process.

In the case of the proposed error compensation method, if gives a good results in improving the accuracy of angular velocity measurement. As is shown in Fig. 10, the real (red) and dotted (blue) lines delegate the input angular velocities of ω_x and ω_y respectively. And the simulation result shows that there is no marked difference in measured results before and after compensation. However, when it comes to the measurement error, the difference becomes significant.

Fig. 11 reveals the effectiveness of the compensation method, the measurement errors in x- and y-direction are compared before and after compensation at different rotor spinning speed Ω.

According to Fig. 11, we can see the measurement errors induced by the centrifugal deformation increased with the rising of the rotor rotation speed both in x- and y-directions. As for the proposed method, the measurement errors are decreased greatly after compensation. The compensation effect in x-direction is superior to y-direction, and at high rotor spinning speed is superior to low speed. At 10000rpm, the peak values of measurement error decreases from 5.8×10^{-4}rad/s before compensation to 0.8×10^{-4}rad/s after compensation in x-direction, approximately 83%. In y-direction, it decreases from 3.4×10^{-3} rad/s before compensation to 2.6×10^{-3} rad/s, approximately 24%. At 5000rpm, the peak values of measurement error decreases from 2.8×10^{-4}rad/s before compensation to 0.5×10^{-4}rad/s after compensation in x-direction, approximately 82%. In y-direction, it decreases from 1.7×10^{-3}rad/s before compensation to 1.3×10^{-3}rad/s, approximately 23%. Because of the low accuracy of the
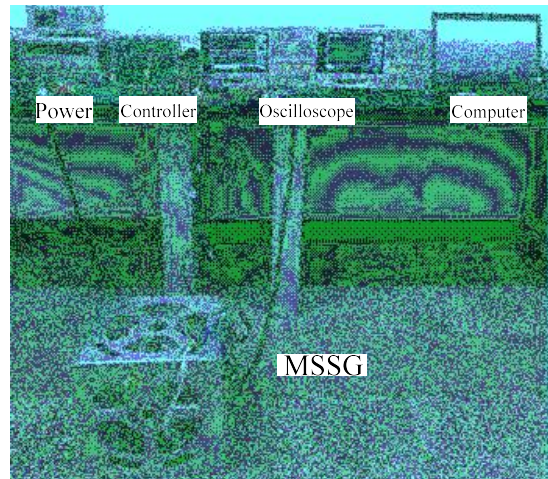

Fig. 12. Experimental setup

MSSG in y-direction for angular measurement, the measurement errors are larger than that in x-direction before and after error compensation, and the improvement of error compensation in y-direction is inconspicuous.

The simulation demonstrates that, the theoretical model for centrifugal deformation of the rotor with dedicated configuration possesses higher accuracy, and the measurement errors produced by the rotor centrifugal deformation have been greatly compensated in both the same axis and orthogonal axis by the proposed method in this paper. The results also show that the error compensation method can come into play in real time, and the compensation effects are not bound by the rotor spinning speed, and the method is easy to practice.
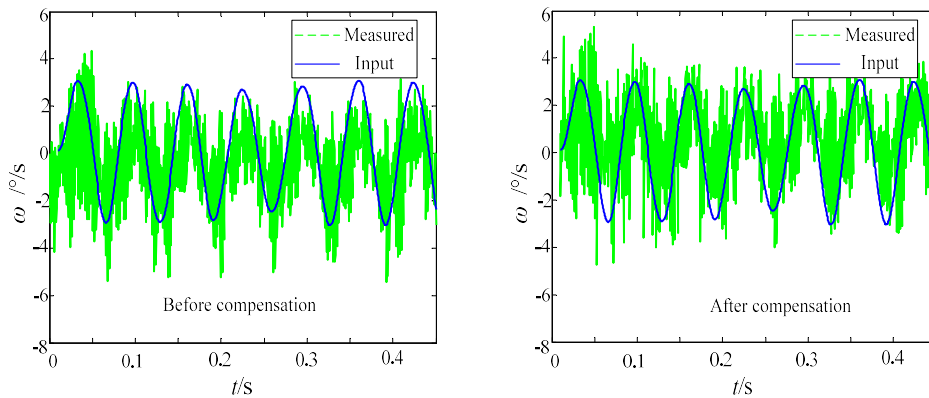
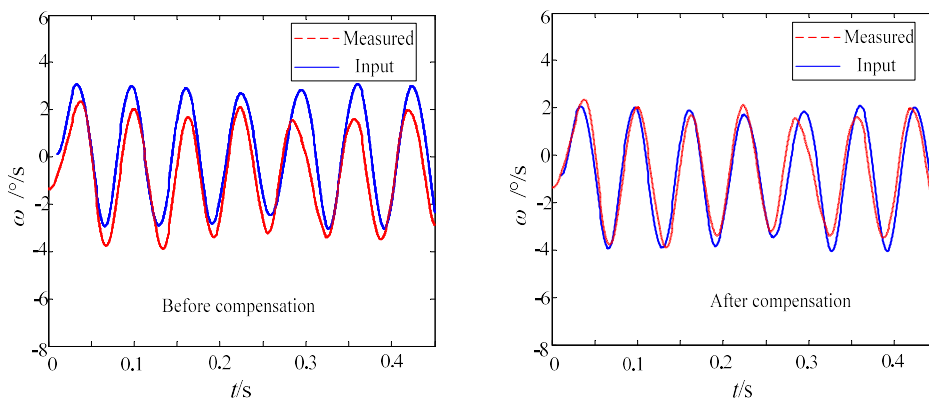**Fig. 13.** Measurement results before and after compensation

Fig. 14. Filtered measurement results before and after compensation

6. Experiment for Error Compensation

The single-axis angular velocity measurement is carried out on the prototype MSSG. The experimental setup is shown in Fig. 12, and the MSSG is fixed on a turntable. The parameters of the MSSG are identical to the parameters shown in Table 1, and the rotation speed is set to 700rpm as the prototype MSSG is unable to rotate at high speed at present.

Fig. 13 indicated the measured angular velocity from the MSSG and the input signal from the turntable in y-axis before and after compensation. And the measurement results by low-pass filtering are shown in Fig. 14.

It is clear that although the measured results include some noise, the measured angular velocities correspond well to the input signals according Fig. 13. And according to Fig. 13 and Fig. 14, we can find that the measurement errors in y-direction have been greatly reduced by the proposed compensation method. Before compensation, the maximal measurement error appears at 0.36s and its value is about 81.3%. As for the proposed method, the maximal error has been decreased to 50.9%, the measurement accuracy of the MSSG has been improved for approximately 30%.

The results confirm the point that the measurement

errors produced by the centrifugal deformation have been greatly compensated by the proposed method in this paper. However, dues to the low rotation speed of the prototype MSSG, the measurement accuracy does not reach the ideal result. Considering the relationship between the centrifugal deformation error and the rotor rotation speed, it is assumed that the proposed compensation method is more effective if the rotation speed rises to 8000-12000 rpm.

7. Conclusion

In this paper, a modeling method of centrifugal deformation error for baroque rotors has been presented. Finite element analysis demonstrates that the relative errors of the proposed method are no more than 15%. And a novel error compensation method based on the modeling method is proposed to improve the accuracy for angular velocity measurement of MSSG. Under various rotor spinning speeds, the validity of the error compensation method was evaluated. Simulations results show that with the proposed compensation method the measurement error can be reduced approximately 83% and 23% in x- and y-direction respectively. Experiment for centrifugal deformation error compensation has been carried on at 700 rpm, and the results demonstrate that

with the proposed compensation method the measurement error can be reduced more than 30%, so that improves the measurement accuracy of angular velocity for a MSSG. In future, the compensating efficiency of the proposed method needs to be investigated and verified further at high rotation speed. To sum up, the presented error compensation method can effectively compensate the measurement error caused by centrifugal deformation in real-time without adding accessory apparatus, realizing its high-precision attitude measurement. The same modeling and compensation methods can be easily extended to other configurations with spinning rotors.

References

[1] Ren Yuan and Fang Jiancheng, "High-precision and Strong-robustness Control for an MSCMG Based on Modal Separation and Rotation Motion Decoupling Strategy," *IEEE Trans. Ind. Electron.*, vol. 61, no. 12, pp. 1539-1551, Dec. 2014.

[2] Tang Jiqiang, Fang Jiancheng, and Wen Wen, "Superconducting Magnetic Bearings and Active Magnetic Bearings in Attitude Control and Energy Storage Flywheel for Spacecraft," *IEEE Trans. Applied Superconductivity*, vol. 22, no. 6, pp. 178-185, Dec. 2012.

[3] Zheng Shiqiang and Han Bangcheng, "Investigations of an Integrated Angular Velocity Measurement and Attitude Control System for Spacecraft Using Magnetically Suspended Double-gimbal CMGs," *Advances in Space Research*, vol. 51, no. 12, pp. 2216-2228, Jun. 2013.

[4] Akiyama Tomohiro, Mizuno Takeshi, Takasaki Masaya, Ishino Yuji and Obara Kyosuke, "Development of a Totally Active Magnetically Suspended Gyro," *Mechatronics*, vol. 24, no. 8, pp. 1059-1070, Jul. 2014.

[5] Li Hai, Liu Xiaowei, Chen Weiping and Zhang Haifeng, "A Miniaturized Two-dof Rotational Gyro with a Ball-joint Supported Permanent Magnet Rotor," *Applied Physics Letters*, vol. 109, no. 1, pp. 013503-1-013503-5, Jul. 2016.

[6] Hu Xinning, Wang Qiuliang, Cui Chunyan, Gao Fei, Wang Hui, Li Yi, Wang Housheng, Cheng Junsheng, Dai Yinming and Yan Luguang, "Torque Compensation System Design for a Spherical Superconduction Rotor," *IEEE Trans. Instrumentation. Measurement*, vol. 63, no. 12, pp. 2789-2794, Dec. 2014.

[7] A. V. Egorov, B. E. Landau, S. L. Levin and S. G. Romanenko, "Rotor Motion in a Strapdown Electrostatic Gyro of an Orbiting Spacecraft," *Gyroscopy and Navigation,* vol. 3, no. 2, pp. 144-151, Apr. 2012.

[8] Yang Hui, Gao Fei, Li Lankai, Cui Chunyan, Hu Xinning, Wang Hui and Wang Qiuliang, "Analysis of superconducting hollow spherical rotor's deformation," *Cryo. & Supercond.*, vol. 43, no. 1, pp. 51-55, Jan. 2015.

[9] Li Yi, Pei Yulong, Song Zaixin and Chai Feng, "Effect of Rotor Deformation on Magnetic Radial Force in Interior Permanent Magnet Synchronous Motors with V-shaped Rotor Structures," *IECON 2016-42ⁿᵈ Annual Conference of the IEEE Industrial Electronics Society*, Firenze, Italy Oct. 2016, pp. 1906-1911.

[10] Katsumi Yamazaki and Yusuke Kato, "Iron Loss Analysis of Interior Permanent Magnet Synchronous Motors by Considering Mechanical Stress and Deformation of Stators and Rotors," *IEEE trans. magnetic*, vol. 50, no. 2, pp. 909-912, Feb. 2014.

[11] Tang Jiqiang and Zhang Yanshun, "High-speed Carbon Fiber Rotor for Superconducting Attitude Control and Energy Storage Flywheel," *2012 3rd International Conference on Digital Manufacturing & Automation*, Guilin, China, Jul. 2012, pp. 477-481.

[12] Zhang Junan, Qiu Changhua, Yan Ming, Wang Yanguo and Mao Yuhui, "Analysis on Hollow Rotor Deformation of Electrostatic Suspended Gyroscope," *Optics and Precision Engineering*, vol. 14, no. 1, pp. 116-120, Jan. 2006.

[13] Liu Ruige, Song Feng and Liu Ruiying, "Deformation Analysis and Optimization on Hollow Spherical Rotor in Electrostactically Suspended Gyroscope," *International Journal of Plant Engineering and Management*, vol. 17, no. 1, pp. 58-64, Jan. 2012.

[14] Sun Xinmin, and Tao Lizhi, "Deformation Design of Long-spherical Hollow Rotor of Electrostatic Suspended Gyroscope," *Optics and Precision Engineering*, vol. 17, no. 9, pp. 2206-2211, Sep. 2009.

[15] Xin Chaojun, Cai Yuanwen, Ren Yuan and Fan Yahong, "Modeling and Analysis of Drift Error from Stator of a MSSG with Double Spherical Envelope Surfaces," *Journal of Electrical Engineering & Technology*, vol. 11, no. 5, pp. 1475-1485, Oct. 2016.

[16] Xin Chaojun, Cai Yuanwen, Ren Yuan, Fan Yahong, Xu Guofeng and Lei Xu, "Analysis, Modeling and Compensation of Dynamic Imbalance Error for a Magnetically Suspended Sensitive Gyroscope," *Journal of Magnetics*, vol. 24, no. 4, pp. 529-536, Oct. 2016.

Chao-Jun Xin He received his B.S., M.S. degrees in aerospace engineering from Equipment Academy, China, in 2003 and 2008, respectively. And he received the Ph.D. degrees from Space Engineering University in 2017. His research interests are guide, navigation and control.

Yuan-Wen Cai He received the B.S. and M.S. degrees in electrical engineering from National University of Defense Technology in 1988 and 1990. And he received the Ph.D. degrees from Beihang University in 2005. He has been a professor in the Department of Space Science and Technology, Space Engineering University. His research interest is aerospace launch and measurement.

Yuan Ren He received his B.S. degree from Ordnance Engineering College in 2003 and the M.S. degree from Jiangsu University in 2007. He received the Ph.D. degree from Beihang University in 2013. His main research interests are in the areas of advanced inertia measurement and control.
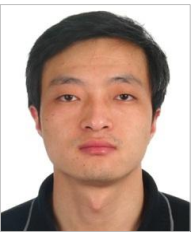
Ya-Hong Fan He received his B.S. degree from Shaanxi University of Technology in 1996. And he received his M.S. and Ph.D. degrees from Beihang University in 2003 and 2011 respectively. His research interests include magnetically suspended control moment gyroscope analysis and design, control and condition monitoring.